JOURNAL OF GEOPHYSICAL RESEARCH, VOL. 115, B05314, doi:10.1029/2009JB006533, 2010

Thermochemical pressurization of faults during coseismic slip

N. Brantut,[1] A. Schubnel,[1] J. Corvisier,[1] and J. Sarout[1,2]

Received 10 April 2009; revised 8 October 2009; accepted 6 January 2010; published 29 May 2010.

[1] During earthquakes, frictional heating on the fault plane induces a temperature rise and thus a pore pressure rise, which is known as thermal pressurization (TP). Coseismic mineral dehydrations may occur because of this temperature increase and are included within the TP framework. Dehydrations are modeled as a source term for pore pressure because of the total volume change and as a sink term for temperature because they are endothermic. The reaction occurs within the slipping zone when a threshold temperature T_s is reached. Dehydration reaction kinetic is modeled using a first-order reaction rate. Using energy and fluid mass conservation, we derive analytically the equations of evolution of pore pressure, temperature, and reaction extent in the undrained, adiabatic case using a constant reaction rate. We investigate the values of the kinetic rate constant required to produce a significant effect, which are much higher than laboratory data reported in the literature on clay, serpentine, and phyllosilicate dehydration. We show, however, that such high values can be reached if the temperature dependency of the rate constant is taken into account. Next, we include fluid and heat transport and use an Arrhenius law to calculate the rate constant as a function of temperature. The subsequent set of differential equations is then solved numerically. The main effect of dehydration reactions is an increase of pore pressure and a stabilization of the temperature during slip. We explore a wide range of parameters in order to determine in which cases dehydration can be considered as a nonnegligible process. For high-permeability rocks ($>10^{-18}$ m^2) and when the amount of water that can be released is of the order of 10%, dehydration is an important mechanism as it delays the onset of melting, which would normally occur even within the TP framework. If the onset temperature is low compared to the initial temperature T_0 ($T_s - T_0 \lesssim 150$°C), overpressure can occur. If the reactions are highly endothermic and if their kinetic is fast enough, frictional melting would not occur unless the dehydration reactions are completed within the slipping zone.

Citation: Brantut, N., A. Schubnel, J. Corvisier, and J. Sarout (2010), Thermochemical pressurization of faults during coseismic slip, *J. Geophys. Res.*, *115*, B05314, doi:10.1029/2009JB006533.

1. Introduction

[2] Although most of our knowledge of earthquakes energy budget comes from the part of the energy that is radiated during an earthquake and can then be observed on seismograms, it is certain that an important part is also dissipated along the fault plane: for example converted into heat within the fault zone or into surface energy within the process and damage zones. However, the fact that field observations of local melting of fault rocks, i.e., pseudotachylytes, are scarce, along with the absence of clear temperature anomaly on the San Andreas Fault led *Sibson* [1973] and *Lachenbruch* [1980] to argue that the presence of fluids within the fault rocks may prevent an important temperature rise: as the faults heats up due to frictional work, the pore pressure builds up and decreases the fault strength, which in turn reduces the frictional heating. This idea was first suggested by *Goguel* [1969], and exhaustive theoretical works have been published on the topic in the past two decades [e.g., *Lachenbruch*, 1980; *Mase and Smith*, 1985; *Andrews*, 2002; *Rice*, 2006; *Rempel and Rice*, 2006; *Sulem et al.*, 2007]. In particular, the relationship between frictional melting and thermal pressurization has already been studied by *Rempel and Rice* [2006].

[3] On the other hand, many experimental studies have highlighted various phenomena that are likely to occur during earthquakes. For instance, laboratory data on natural fault gouges suggest that thermal pressurization could indeed play an effective role during real earthquakes [*Wibberley and Shimamoto*, 2003; *Noda and Shimamoto*, 2005; *Wibberley and Shimamoto*, 2005]. So could local melting [*Tsutsumi and Shimamoto*, 1997; *Hirose and Shimamoto*, 2005; *Di Toro et al.*, 2006] and silica gel formation in quartz rocks

[1] Laboratoire de Géologie, CNRS UMR 8538, École Normale Supérieure, Paris, France.
[2] Now at CSIRO Division of Petroleum Resources, Kensington, Western Australia, Australia.

0148-0227/10/2009JB006533

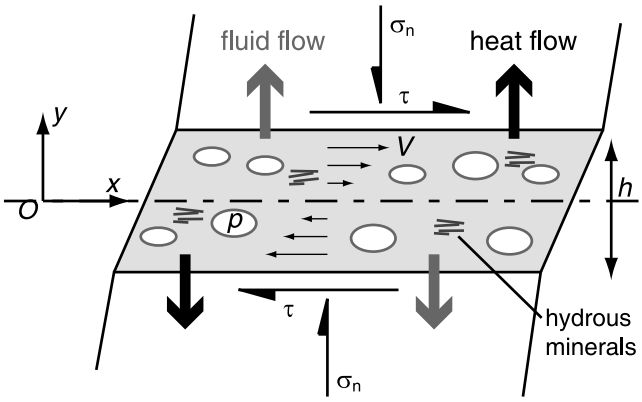

Figure 1. Sketch of the fault zone model. The slipping zone thickness is *h*. Diffusion of heat and fluid occurs perpendicular to the fault direction. Hydrous minerals are present within the slipping zone and may dehydrate at elevated temperature.

[*Goldsby and Tullis*, 2002], which have been produced in the laboratory. Recently, coseismic mineral decompositions such as dehydration of serpentinite or kaolinite [*Hirose and Bystricky*, 2007; *Brantut et al.*, 2008] and decarbonation of calcite and siderite [*Han et al.*, 2007b, 2007a] have also been demonstrated experimentally. Most importantly, field evidences that such reactions may take place coseismically have already been presented in the Chelung-Pu drill cores by *Hirono et al.* [2008]; *Hamada et al.* [2009], and in the Nojima fault core where evidence of carbonate degassing were observed by *Famin et al.* [2008].

[4] If they occur during an earthquake, dehydration reactions are likely to influence the mechanical behavior of fault during slip in many geological settings since most shallow to intermediate depth fault gouges are rich in clay minerals such as illite, smectite, montmorillonite, kaolinite (e.g., in the San Andreas or Aegion faults [*Solum et al.*, 2006; *Sulem et al.*, 2004]) which can dehydrate at temperatures that can well be attained during thermal pressurization (e.g., using the values suggested by *Rempel and Rice* [2006]). In consequence and contrary to local melting, both phenomena (thermal pressurization of pore fluid and dehydration reactions) are likely not to be exclusive, as suggested in a recent publication [*Brantut et al.*, 2008]. In fact, a recent study by *Sulem and Famin* [2009] has already shown the influence of coseismic decarbonation of limestone on the thermomechanical properties of faults.

[5] Following these recent observations, we present here a new formulation of thermal pressurization in which we implemented a chemical coupling in order to take into account mineral reactions such as dehydrations. This coupling takes place after the onset of dehydration, within the thermal pressurization framework, and we calculate the subsequent pore pressure and temperature evolutions within a thin, water-saturated slipping zone. First, we present our new formulation of the thermal pressurization equations which includes the dehydration source terms in the poroelastic coupling as (1) a water mass transfer from the solid phase to the fluid phase and (2) a modified energy balance equation because mineral dehydrations are generally endothermic reactions and may thus represent an important energy sink (as noted by *Sulem and Famin* [2009]). Second, we solve this set of coupled equations analytically in the adiabatic, undrained case with a constant reaction kinetic. Using the results of these calculations performed at constant rate, we discuss the effect a different rate would have, as well as the effect of its dependency on temperature. Finally, we solve numerically the system of equations and explore the model behavior for different sets of parameters: (1) we test the parameters linked to the reaction itself such as the kinetic of the reaction, its activation energy, the enthalpy variation due to the reaction and the equilibrium temperature at which the reaction takes place, and (2) the parameters linked to the fault rock properties such as the slipping zone thickness, the fault rock permeability and the depth at which the slip occurs. In each of these cases, the effects of the chemical reaction on temperature and pressure are investigated in comparison to what would be observed in the regular thermal pressurization framework (i.e., with no dehydration).

2. Description of the Model

2.1. Thermal Pressurization With Dehydration

[6] Thermal pressurization (TP) can be modeled by coupling heat diffusion equations and poroelasticity equations [*Lachenbruch*, 1980; *Mase and Smith*, 1985; *Andrews*, 2002; *Rice*, 2006; *Rempel and Rice*, 2006]. Here we derive the TP equations including a chemical coupling as source terms in the mass and energy conservation equations. The fault main slipping zone is considered as a porous, elastic, fluid saturated medium; fluid and heat transfers occur perpendicularly to the fault (coordinate y) only. For the sake of simplicity, variations of the parameters along the fault are not taken into account, so the problem is fully one-dimensional. Figure 1 is a sketch representing the physical setting of the problem. In order to develop the model in its most general form, we do not focus here on any particular dehydration reaction. It is only assumed here that the reactions are temperature dependent; that is, they start at a threshold temperature T_s independent of the stress or pore pressure applied in the medium. This assumption appears to be reasonable since we focus on the shallow part of the crust (<15 km), where the lithostatic pressure and the pore pressure are of the order of several hundreds megapascals: in this range of pressure, the phase transition of most of the hydrous minerals (clays and phyllosilicates) is almost not pressure dependent. This starting temperature is not necessarily the equilibrium temperature: the heating rate is very high and there might be a temperature overstep. In the simplest case, dehydration reactions can be thought of as

$$\text{Mineral 1} \rightarrow \text{Mineral 2} + \nu H_2O, \tag{1}$$

where ν is the number of moles of water that are released during the reaction.

[7] To keep the spirit of making elementary estimates, the assumption is made that the reaction occurs within the slipping zone only. Such an hypothesis is reasonable since (1) TP always produces higher temperatures inside the slipping zone and (2) there might be a mechanical activation of the mineral reaction by grain crushing [*Makó et al.*, 2001; *Horváth et al.*, 2003] during shearing, which could facilitate

the dehydration. The enthalpy variation of the reaction is denoted by $\Delta_r H$. To keep a general form for the calculations, it is convenient to define χ as the mass fraction of water that can be released per unit of total rock mass:

$$\chi = w_m \frac{\nu M_{H_2O}}{M_m}, \tag{2}$$

where M_m and M_{H_2O} are the molar weight of the dehydrating mineral and of the fluid, respectively, and w_m is the mass fraction of the dehydrating mineral in the rock. The total energy change per unit volume of the slipping layer ΔH can then be expressed as

$$\Delta H = \chi \frac{\rho}{\nu M_{H_2O}} \Delta_r H, \tag{3}$$

where ρ is the bulk density of the rock. Assuming that all the frictional work is converted into heat, the energy equation in the slipping zone is given by

$$\rho c \frac{\partial T}{\partial t} = \tau \dot{\gamma} - \frac{\partial q_{th}}{\partial y} + \Delta H \frac{\partial \xi}{\partial t}, \tag{4}$$

where τ denotes the shear stress applied on the fault, $\dot{\gamma}$ the shearing rate, q_{th} the heat flux, ξ the extent of reaction, c the specific heat capacity per unit of rock mass. The heat flux can be expressed using Fourier's law: $q_{th} = -K\partial T/\partial y$ for pure conduction, where K is the thermal conductivity. The shearing rate in a layer of thickness h for a slip rate V is $\dot{\gamma} = V/h$. The shear stress is calculated as the frictional resistance of the layer, proportional to the average effective stress in the slipping zone: $\tau = \mu\,(\sigma_n - \overline{p})$, where μ is the friction coefficient, σ_n the normal stress applied on the fault and $\overline{p}$ the average pore pressure whithin the layer. Thus the heat equation becomes

$$\frac{\partial T}{\partial t} = \mu(\sigma_n - \overline{p}) \frac{V}{h\rho c} + \alpha_{th} \frac{\partial^2 T}{\partial y^2} + \frac{\Delta H}{\rho c} \frac{\partial \xi}{\partial t}, \tag{5}$$

where $\alpha_{th} = K/\rho c$ the thermal diffusivity, which is assumed to be spatially constant, and independent from both pressure and temperature. ΔH can be negative if the reaction is endothermic or positive if the reaction is exothermic. It is possible to define the theoretical temperature change due to the reaction by

$$\Delta T^d = \frac{\Delta H}{\rho c}, \tag{6}$$

which corresponds to the contribution of the chemical reaction to the temperature evolution. Most dehydration reactions being endothermic, the sign of ΔT^d is negative and the temperature will decrease as the reaction progresses. The relative importance of friction versus dehydration will be discussed later.

[8] The mass conservation equation for the fluid in the slipping zone is

$$\frac{\partial m}{\partial t} + \frac{\partial q_f}{\partial y} = \frac{\partial m^d}{\partial t}, \tag{7}$$

where m is the fluid mass per unit volume, q_f is the fluid flux and m^d is the fluid mass per unit volume coming from dehydration. The fluid mass increment dm can be written as [*Rice*, 2006]

$$dm = \rho_f \beta^* \left(dp - \Lambda dT + \frac{dn^{irr}}{\beta^*} \right), \tag{8}$$

where n is the porosity, ρ_f the fluid density, n^{irr} the irreversible (inelastic) deformation of pores. Λ and β^* are defined as follows:

$$\Lambda = \frac{\lambda_f - \lambda_n}{\beta_f + \beta_n}, \tag{9}$$

$$\beta^* = n(\beta_f + \beta_n), \tag{10}$$

where β_n is the pore compressibility, λ_n the pore thermal expansivity, β_f the fluid compressibility and λ_f the fluid thermal expansivity. The source term due to dehydration in equation (7) is simply

$$dm^d = \rho \chi d\xi. \tag{11}$$

The reaction is also associated with a volume change, considered here as an irreversible variation of porosity Δn^{irr}. The increment of porosity can thus simply be expressed as a function of ξ:

$$dn^{irr} = \Delta n^{irr} d\xi. \tag{12}$$

[9] The fluid flux q_f can be expressed by Darcy's law:

$$q_f = -\rho_f \frac{k}{\eta_f} \frac{\partial p}{\partial y}, \tag{13}$$

where k is the permeability and η_f is the fluid viscosity. Substituting Darcy's law and equations (8), (11), and (12) into mass conservation equation (7) yields

$$\frac{\partial p}{\partial t} = \Lambda \frac{\partial T}{\partial t} + \frac{1}{\rho_f \beta^*} \frac{\partial}{\partial y} \left(\rho_f \frac{k}{\eta_f} \frac{\partial p}{\partial y} \right) + \left(\frac{\rho}{\rho_f} \chi - \Delta n^{irr} \right) \frac{1}{\beta^*} \frac{\partial \xi}{\partial t}. \tag{14}$$

Aside from the thermal effect, such an expression is similar to the equation of *Wong et al.* [1997] for dehydrating systems. Except for the additional terms $[(\rho/\rho_f)\,\chi - \Delta n^{irr}]\,(1/\beta^*)\,(\partial\xi/\partial t)$ and $(\Delta H/\rho c)(\partial\xi/\partial t)$, the calculations lead to the standard equations of thermal pressurization [e.g., *Rice*, 2006]. These additional terms depend on (1) the dehydration kinetic $(\partial\xi/\partial t)$, (2) the amount of water that can be released χ, and (3) the solid volume change Δn^{irr}. The pore pressure variation induced by the reaction can be expressed as follows:

$$\Delta p^d = \left(\chi \frac{\rho}{\rho_f} - \Delta n^{irr} \right) \frac{1}{\beta^*}. \tag{15}$$

This expression is general and does not depend on the dehydration mechanism. The water that is released can be either bonded, adsorbed or interlayered (in the case of clays such as illite-smectite). The density of the fluid ρ_f has to be calculated as a function of pressure and temperature because the fluid can become supercritical during thermal pressuri-

Table 1. Data Used for the Adiabatic, Undrained Model

Parameter	Symbol	Value	Units
Friction coefficient	μ	0.4	
Specific heat capacity per unit volume	ρc	2.7	MPa °C^{-1}
Thermal expansion of pores[a]	λ_n	0.02×10^{-3}	°C^{-1}
Compressibility of pores	β_n	2.49×10^{-9}	Pa^{-1}
Thermal expansion of water	λ_f	1.21×10^{-3}	°C^{-1}
Compressibility of water[a]	β_f	0.88×10^{-9}	Pa^{-1}
Density of water	ρ_f	800	kg m^{-3}
Slip velocity	V	1	m.s^{-1}
Normal stress	σ_n	196	MPa
Initial pore pressure	p_0	70	MPa
Initial temperature	T_0	210	°C
Slipping zone thickness	h	1	mm
Porosity	n	0.05	
Equilibrium temperature	T_s	500	°C
Enthalpy of reaction	$\Delta_r H$	100	kJ mol^{-1}
Mass fraction of water	χ	0.01	
Characteristic time of thermal pressurization	t_{tp}	0.0192	s
Onset time of dehydration	t_s	$1.19 \times t_{tp}$	s
Characteristic time of energy-controlled kinetic	t_c	$0.063 \times t_{tp}$	s
Virtual temperature change	ΔT^d	−35.7	°C
Virtual pressure change	Δp^d	208	MPa

[a]The constant values of thermal expansion and compressibility of pores and water come from *Rice* [2006].

zation. Thermal pressurization of typical fault materials at depth (e.g., using the parameters summarized in Table 2) induces a relatively high temperature increase, up to several hundreds of degrees, whereas the fluid pressure is bounded by the normal stress applied on the fault, which is of the order of 100 MPa at 4 km depth. In such a case, the density of water is relatively low, thus promoting a positive value of Δp^d. For instance, a thermodynamic calculation performed with the software GE0TAB [*Berman*, 1991, 2007] for the dehydration of pure chrysotile at a pore pressure of 200 MPa and a temperature of 600°C yields a net increase of volume of about +24.7%.

2.2. Representative Parameters

[10] The set of the thermoporomechanical parameters used in TP calculations is not fully investigated here. As our approach consists in giving a broad view of the coupling phenomena, we do not focus on a particular fault zone, but rather choose a representative set of parameters in order to observe the variety of processes triggered by the newly introduced couplings. Based on field and experimental data in the literature [*Wibberley*, 2002; *Wibberley and Shimamoto*, 2003; *Noda and Shimamoto*, 2005; *Mizoguchi*, 2005] and on the parameter set used by *Rice* [2006] and *Rempel and Rice* [2006], we choose the values that are presented in Tables 1 and 2. Such values correspond to a typical clay bearing, low porosity, low permeability ultracataclasite, as can be observed in exhumed faults such as the Median Tectonic Line (SW Japan) [*Wibberley*, 2002; *Wibberley and Shimamoto*, 2003; *Brantut et al.*, 2008] or the Hanaore Fault (SW Japan) [*Noda and Shimamoto*, 2005]. The slipping zone thickness is set to 1 mm, the porosity to 5% and the permeability to 10^{-20} m^2, corresponding to typical values for natural fault gouges [*Wibberley and Shimamoto*, 2003; *Noda and Shimamoto*, 2005; *Sulem et al.*, 2007]. The pore compressibility and the thermal expansion coefficient correspond to average values for a highly damaged rock [*Rice*, 2006]. For simplicity, the dependency of the fault rock physical parameters (mainly porosity and permeability) with effective pressure is not taken into account. The depth is set at about 7 km, which leads to a average normal lithostatic stress of about 196 MPa and an average hydrostatic fluid pressure of 70 MPa. The initial temperature is 210°C, corresponding to a geotherm of 30° km^{-1}. The frictional coefficient is set at an average value of 0.4 [*Noda and Shimamoto*, 2005], following laboratory data on the Median Tectonic Line (MTL) fault gouge [*Brantut et al.*, 2008] and the Nojima fault gouge [*Mizoguchi*, 2005]. According to recent studies [*Han et al.*, 2007b, 2007a; *Brantut et al.*, 2008; *Mizoguchi et al.*, 2009], it would be reasonable to let the friction coefficient itself evolve with displacement and/or temperature; however, there is still no consensus in the literature regarding the rheology to be used for describing its evolution, and such considerations are beyond the scope of this study.

[11] The water properties are either set at their initial values at depth (for the analytical solution developed later on), or calculated as functions of p and T using GEOTAB and the IAPWS-IF97 (International Association for the Properties of Water and Steam, Industrial Formulation 1997) data sets.

[12] In addition to this set of thermoporomechanical parameters, our model introduces new parameters linked to the chemistry and mineralogy of the rock. Because these parameters are either poorly constrained or strongly dependent on the particular mineral, a basic set of parameters is chosen to match a typical clay or phyllosilicate (such as kaolinite), and the dependency of the solution on these parameters will be extensively investigated. The water content χ can be calculated knowing the mineralogy and the particular dehydration reaction involved (equation (2)). The solid volume change Δn^{irr} also depends on each specific chemical reaction. In general, the total volume change is positive, and we never deal with negative pore pressure changes. This parameter can be ignored by assuming that a nonnegligible value of Δn^{irr} can be taken into account by setting a lower value of χ. This is an approximation because the porosity also influences the storage capacity and thus the transport properties of the rock, but the model presented here neglects these changes. This hypothesis will be discussed later. The temperature T_s at which dehydration starts is set at 500°C: this can be viewed as an average for most clays and hydrous phyllosilicates. Depending on the mineral, this temperature can vary from 300°C (smectite) to 800°C (chlorite). As stated in section 2.1, these values should not correspond to the real thermodynamic equilibrium, but rather to a temperature overstep at which the reaction becomes significant. This will be fully discussed in section 4. The enthalpy variation $\Delta_r H$ is well constrained by laboratory data and most of the values can be precisely calculated with the thermodynamic calculation software GEOTAB [*Berman*, 1991, 2007]. A value of ~1000 kJ mol^{-1} corresponds roughly to an upper bound for most of dehydration reactions. Representative values are reported in Table 3. The value for $\Delta_r H$ will be set in the range 10–1000 kJ mol^{-1}. As shown in equation (3), the stochiometry of the reaction is also involved to calculate ΔH as a function of χ. An average of $\nu \approx 2$ is taken, thus implying $\Delta H \approx \chi \times 10^9$ to $\chi \times 10^{11}$.

Table 2. Data Used in the Numerical Calculations

Parameter	Symbol	Value	Units
Friction coefficient	μ	0.4	
Specific heat capacity per unit volume	$\rho\, c$	2.7	MPa °C^{-1}
Thermal diffusivity	α_{th}	1	mm^2 s^{-1}
Thermal expansion of pores[a]	λ_n	0.02×10^{-3}	°C^{-1}
Compressibility of pores[a]	β_n	2.49×10^{-9}	Pa^{-1}
Thermal expansion of water[b]	λ_f		°C^{-1}
Compressibility of water[b]	β_f		Pa^{-1}
Density of water[b]	ρ_f		kg m^{-3}
Viscosity of water[c]	η_f		Pa s
Slip velocity	V	1	m s^{-1}
Normal stress	σ_n	196	MPa
Initial pore pressure	p_0	70	MPa
Initial temperature	T_0	210	°C
Slipping zone thickness	h	1	mm
Porosity	n	0.05	
Permeability	k	10^{-20}	m^2
Equilibrium temperature	T_s	500	°C
Rate constant at T_s	κ_s	10^{-4}	s^{-1}
Enthalpy of reaction	$\Delta_r H$	100	kJ mol^{-1}
Activation energy	E_a	300	kJ mol^{-1}

[a]Pores compressibility values β_n and pores thermal expansion values λ_n come from *Rice* [2006].
[b]Thermodynamic properties of water are calculated with GE0TAB software.
[c]Water viscosity is calculated with a polynomial fit of IAPWS-IF97 data.

Note, however, that this value could be precisely calculated when considering a particular chemical reaction.

3. Analytical Solution for the Adiabatic, Undrained Case With Constant Kinetic Parameters

[13] In order to give an insight on the thermal, chemical and mechanical couplings described above, we first consider the case where heat and fluid transports are negligible. The case of TP without chemical couplings has been completely solved by *Lachenbruch* [1980] (among many others), leading to the following equations for pressure and temperature:

$$T(t) = T_0 + \frac{\sigma_n - p_0}{\Lambda}\left(1 - e^{-t/t_{tp}}\right), \tag{16}$$

$$p(t) = \sigma_n - (\sigma_n - p_0)e^{-t/t_{tp}}, \tag{17}$$

where $t_{tp} = \rho ch/(\Lambda\mu V)$ is the characteristic thermopressurization weakening time. In this situation, there is no dependency on the spatial coordinate y, so strictly $T = \overline{T}$ and $p = \overline{p}$. In our case, this description remains valid until the temperature reaches T_s and the reaction starts. This corresponds to a time t_s and a pore pressure $p_s = p_0 + \Lambda(T_s - T_0)$.

3.1. Energetically Constrained Reaction Rate

[14] At this point, the reaction starts and a governing law is needed for the reaction rate. As a first approximation, we may consider that starting from t_s, all the frictional energy is absorbed by the reaction rather than converted into heat. In other words, the energy produced by the action of shear stress is dissipated into latent heat of reaction and does not directly increase the temperature. For simplicity, a shifted timescale $t^* = t - t_s$ is used in the following.

[15] In such a case, recalling that adiabatic conditions are assumed, the reaction progress can be written as

$$\frac{\partial \xi}{\partial t^*} = -\frac{\mu V(\sigma_n - p)}{\rho ch\Delta T^d}. \tag{18}$$

The differential system for p and T then becomes

$$\frac{\partial T}{\partial t^*} = 0, \tag{19}$$

$$\frac{\partial p}{\partial t^*} = \Delta p^d\left(-\frac{\mu V(\sigma_n - p)}{\rho ch\Delta T^d}\right), \tag{20}$$

which can be directly solved to give

$$T\left(t^*\right) = T_s, \tag{21}$$

$$p\left(t^*\right) = (\sigma_n - p_s)e^{-t^*/t_e}, \tag{22}$$

$$\xi\left(t^*\right) = \frac{\sigma_n - p_s}{\Delta p^d}\left(1 - e^{-t^*/t_e}\right), \tag{23}$$

where $t_e = -t_{tp}\Lambda\Delta T^d/\Delta p^d$ corresponds to the characteristic time of the reaction progress for an energetically constrained kinetic.

[16] The comparison of this characteristic time t_e to the characteristic time of TP t_p gives a straightforward insight of the importance of the dehydration phenomenon compared to TP. Using the parameters summarized in Table 1, we get $t_e/t_r \sim 10^{-2}$, which means that the reaction progresses much faster than TP and is thus a nonnegligible process.

[17] The gray dashed curves on Figure 2 display the evolution of pore pressure, temperature and reaction extent as a function of time. The calculated value of t_e is of the order of 10^{-4} s, which corresponds to a nearly instantaneous reaction.

[18] In this situation, the temperature remains constant during the whole reaction. The pore pressure tends asymptotically to σ_n as the dehydration progresses. The reaction is not complete and ξ is bounded by $\xi_{max} = (\sigma_n - p_s)/\Delta p^d$.

[19] For a higher $|\Delta T^d|$ and/or a lower Δp^d, the characteristic time t_e would be higher but not by more than one order

Table 3. Examples of Mineral Dehydration Reactions

Mineral Reaction	$\Delta_r H$ (kJ mol^{-1})
Kaolinite → quartz + kyanite + 2 water	74[a]
Five chrysotile → talc + 6 forsterite + 9 water	415[a]
Antigorite → 4 talc + 18 forsterite + 27 water	1181[a]
Kaolinite → metakaolinite + 2 water	≈1000[b]

[a]The value of enthalpy variation is calculated using GEOTAB [*Berman*, 1991, 2007], at $T = 600$°C and $P = 200$ MPa, in a water-saturated medium.
[b]This value is taken from *L'vov and Ugolkov* [2005], in standard conditions of P and T.

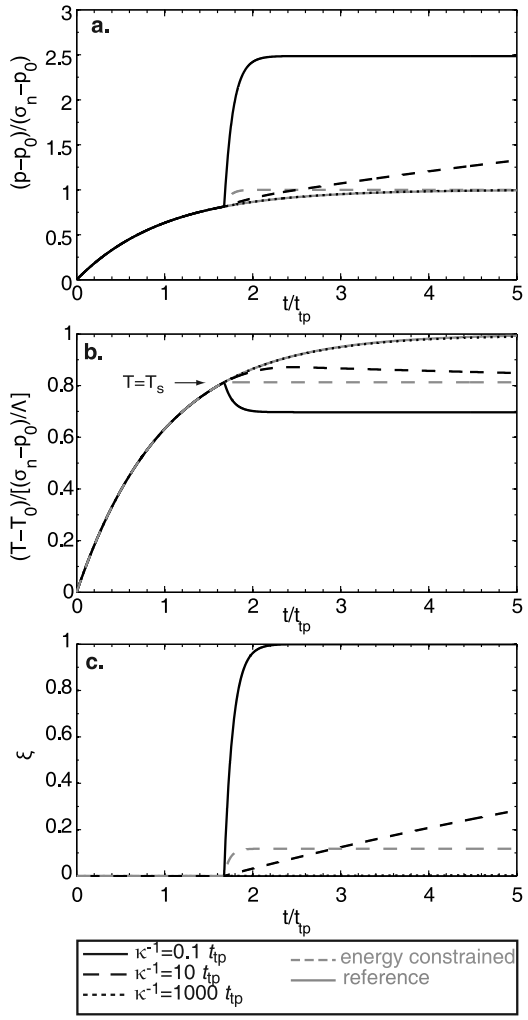

Figure 2. Adiabatic, undrained limit with constant kinetic parameters. (a) Evolution of the pore pressure normalized to $\sigma_n - p_0$. (b) Evolution of the temperature normalized to $(\sigma_n - p_0)/\Lambda$. (c) Reaction extent. The starting temperature is 450°C. The gray curve displays the behavior without dehydration reaction. The gray dashed line corresponds to the case of an energetically constrained reaction rate. The black lines correspond to three different rate constants κ. A fast reaction rate produces a sudden, high overpressure and a drop of temperature. A very slow reaction rate does not change the behavior. An intermediate reaction rate produces a progressive increase of pore pressure, while temperature slightly decreases after a small overstep.

of magnitude. Such reaction rates at the onset of dehydration are probably too fast and more realistic kinetic parameters have to be investigated.

3.2. Solution Using a First-Order Kinetic

[20] Alternatively, we can assume a first-order kinetic to describe the reaction progress:

$$\frac{\partial \xi}{\partial t} = (1-\xi)\kappa, \tag{24}$$

where κ is the rate constant of the reaction, expressed in s^{-1}. The system of equations (5) and (14) can then be solved analytically.

[21] Before going into details, one can notice that in the case when $1/\kappa \gg t_{tp}$, the dehydration reaction occurs much slower than the TP process, which implies that it can be neglected at the timescale of a rapid slip event. In the case when $1/\kappa \lesssim t_{tp}$ both phenomena have to be considered.

[22] The evolution of the reaction progress as a function of time t^* can be directly calculated:

$$\xi\left(t^*\right) = 1 - e^{-t^*/t_r}, \quad \text{thus} \quad \frac{\partial \xi}{\partial t}\left(t^*\right) = \kappa e^{-t^*/t_r}, \tag{25}$$

where $t_r = 1/\kappa$ is the characteristic time of the reaction progress. The evolutions of pore pressure and temperature can then be written

$$\frac{\partial T}{\partial t} = \frac{V\mu(\sigma_n - p)}{\rho c h} + \Delta T^d \kappa e^{-t^*/t_r}, \tag{26}$$

$$\frac{\partial p}{\partial t} = \Lambda \frac{\partial T}{\partial t} + \Delta p^d \kappa e^{-t^*/t_r}. \tag{27}$$

This system of equations can be solved to give

$$T - T_s = \left(\frac{\sigma_n - p_s}{\Lambda} + \frac{\Delta T^d + \Delta p^d/\Lambda}{t_r/t_{tp} - 1}\right)\left(1 - e^{-t^*/t_{tp}}\right) + \left(\Delta T^d + \frac{\Delta T^d + \Delta p^d/\Lambda}{t_{tp}/t_r - 1}\right)\left(1 - e^{-t^*/t_r}\right), \tag{28}$$

$$\sigma_n - p = (\sigma_n - p_s)e^{-t^*/t_{tp}} + \frac{\Lambda \Delta T^d + \Delta p^d}{t_r/t_{tp} - 1}\left(e^{-t^*/t_{tp}} - e^{-t^*/t_r}\right). \tag{29}$$

In both equations (28) and (29), the chemical term (with its characteristic time t_r) appears linked to the porothermomechanical term (with its characteristic time t_{tp}). When the mineral dehydration occurs, both terms act in opposite ways.

[23] Representative examples are plotted on Figure 2, which displays the evolution of pore pressure, temperature and reaction extent as functions of time. The black lines correspond to three different values of t_r, ranging from $10^{-3}\, t_{tp}$ to $10 t_{tp}$. The parameter values used for these simulations are presented on Table 1.

[24] Equations (28) and (29) point out the relative importance of the two characteristic times t_{tp} and t_r. If $t_{tp} \ll t_r$, dehydration can be neglected and the equations can be simplified to give the same system as equations (16) and (17). This is shown by the dotted black curve on Figure 2 which corresponds to $t_r = 10^3 t_{tp}$: it does not show any quantitative difference with the reference case (no dehydration).

[25] For faster reaction rates, i.e., when $t_r = 10\ t_{tp}$ (black dashed curve on Figure 2), the dehydration reaction induces a progressive increase of the pore pressure along with a stabilization of the temperature slightly above T_s. The pore pressure increases beyond the normal stress σ_n, showing that coseismic shear-induced dehydrations can produce transient

overpressures within the slipping zone. In this case, the branch of the curve above σ_n is calculated with no frictional heating.

[26] In the case when $t_r \ll t_{tp}$, dehydration is the dominant mechanism and the system can be rewritten simply as

$$T - T_s \sim \Delta T^d \left(1 - e^{-t^*/t_r}\right), \tag{30}$$

$$p - p_s \sim \left(\Lambda \Delta T^d + \Delta p^d\right)\left(1 - e^{-t^*/t_r}\right). \tag{31}$$

In this situation, the maximum pore pressure rise is $\Delta p^d + \Lambda \Delta T^d$, and does not involve σ_n. The pore pressure can thus increase beyond the normal stress. The full black curve on Figure 2a, calculated with $t_r = 10^{-1} t_{tp}$, highlights this process. It implies that the fault could experience tensile stress: in such situations, various phenomena can occur (hydrofracturing, fluidization), which are beyond the scope of this study.

[27] As explained previously, $\Delta T^d < 0$. From equation (30), the temperature T decreases rapidly down to $T_s + \Delta T^d$, which can be observed on Figure 2b. At this point, the enthalpy change of the reaction needs to be taken into account: if $|\Delta H|$ is large, $|\Delta T^d|$ is also large and the temperature would drop down below the thermodynamic equilibrium temperature of the reaction; that is, the reaction absorbs more energy than that available in the system, which is unrealistic. This highlights the importance of taking into account the energy sink when calculating the kinetic of the reaction in such situations.

3.3. Outcomes and Limitations of the Model

[28] With these calculations on a simplified model, the different behaviors of the system can already be distinguished: (1) when the reaction rate is slow compared to the characteristic time of TP, the dehydration phenomenon can be neglected; and (2) when the reaction occurs over the same timescale as TP, dehydration is not negligible. In the latter case, two situations are possible. If the kinetic constant and/or the enthalpy change are relatively small, the dehydration reaction triggers an additional pore pressure increase that can exceed the normal stress applied on the fault, and concurrently the temperature will slightly decrease below the starting temperature. If the kinetic constant and/or the enthalpy change is large, then the reaction rate is controlled by the amount of energy available in the system rather than by its intrinsic kinetic. In such a case, the temperature is bounded by the starting temperature and a transient equilibrium is met between the energy released mechanically and the energy dissipated by the mineral reaction once the reaction has started and until it is completed.

[29] By combining these different cases, the reaction rate can be rewritten as

$$\frac{\partial \xi}{\partial t} = \min\left\{(1-\xi)\kappa, -\frac{1}{\Delta H}\frac{\mu V(\sigma_n - \overline{p}(t))}{h}\right\}. \tag{32}$$

A high value of enthalpy variation ΔH would promote an energy-controlled kinetic, slowing down the dehydration process. The thickness of the slipping zone h plays a key role because it controls the temperature rise and thus the characteristic time of TP. In consequence, a change in h influences the growth of the pore pressure due to dehydration: a thick slipping zone implies a larger effect of the dehydration source term, whereas a thin slipping zone tends to decrease the relative importance of dehydration compared to TP.

[30] An essential point is that the different behaviors are fundamentally dependent on the reaction kinetic, in particular the value of the kinetic constant κ.

4. Toward a Realistic Reaction Kinetic

[31] In all the calculations so far we have only used constant values for κ during the dehydration process. It is, however, well known that the value of the reaction constant changes with temperature, following an Arrhenius law of the form

$$\kappa(\overline{T}) = \kappa_s \exp\left(\frac{E_a}{R}\left(\frac{1}{T_s} - \frac{1}{\overline{T}}\right)\right), \tag{33}$$

where E_a is an activation energy, κ_s is the rate constant at the starting temperature and R the gas constant. The average temperature $\overline{T}$ within the slipping zone may exceed temporarily the starting temperature because the reaction is not instantaneous and the frictional source term $[\mu(\sigma_n - \overline{p})V\}]/h\rho c$ can be larger than the chemical sink term $(\Delta H/\rho c)(\partial\xi/\partial t)$. The reaction kinetic will accelerate when $\overline{T}$ overshoots the starting temperature T_s. Arrhenius law is valid only at or near equilibrium; a more complete description would include the temperature dependency within E_a, which corresponds to the distance to equilibrium. In fact E_a increases when the temperature exceeds equilibrium, thus increasing exponentially the rate constant κ. As we include only one dependency on temperature in our model, it gives a lower bound estimation of the dehydration kinetic. The validity of our model depends on the maximum overshoot $\overline{T}_{max} - T_s$, and a large difference $\overline{T}_{max} - T_s$ indicates that the reaction would have progressed faster than predicted.

[32] It is important to discuss and choose carefully the values of E_a and κ_s that will be used in the calculations. Laboratory data can be used to constrain these values, despite the fact that they were obtained close to equilibrium or for relatively slow heating rates, which is obviously not the case in fault zones during rapid slip. In the case of dehydration reaction of powdered lizardite at zero effective pressure, the rate constant at 550°C is of the order of 10^{-4} s^{-1}, and the activation energy is approximatively 429 kJ mol^{-1} [*Llana-Fúnez et al.*, 2007]. For kaolinite dehydration, the early work by *Kissinger* [1956] yielded $\kappa(T = 500°C) \approx 2.05 \times 10^{-4}$ to 4.42×10^{-1} s^{-1} and $E_a \approx 100 - 167$ kJ mol^{-1}, depending on the mineral quality and the heating rate. A more recent work on kaolinite by *Bellotto et al.* [1995] gives $\kappa(T = 500°C) \approx 8.8 \times 10^{-5}$ s^{-1} and $E_a \approx 160$ kJ mol^{-1}. For talc dehydration [*Bose and Ganguly*, 1994], we determined $\kappa(T = 800°C) \approx 1.5 \times 10^{-4}$ s^{-1}, using $E_a \approx 372$ kJ mol^{-1}. These authors also show that the reaction rate increases with decreasing grain size (down to 1 μm). In their study, *Bose and Ganguly* [1994] also indicate that the dehydration mechanism of hydrous phyllosilicates would follow a heterogeneous nucleation and growth mechanism, with a narrow activation energy range of

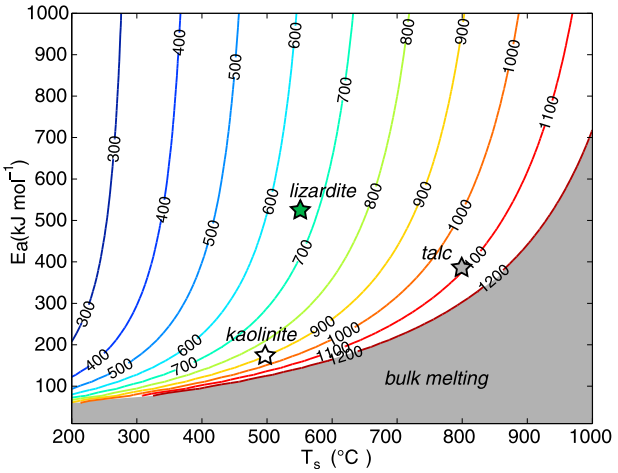

Figure 3. Temperature at which $\kappa(T) = 1$ s^{-1}, for $\kappa_s = 10^{-4}$ s^{-1}, as a function of the activation energy E_a and starting temperature T_s. The calculation uses the Arrhenius law (equation (33)). Data on kaolinite, lizardite and talc come from *Bellotto et al.* [1995], *Llana-Fúnez et al.* [2007], and *Bose and Ganguly* [1994]. The melting temperature of the bulk rock is set at 1200°C.

325–400 kJ mol^{-1}. In addition, numerous studies have investigated dehydration reactions kinetics of kaolinite [e.g., *Yeskis et al.*, 1985; *Klevtsov et al.*, 1988; *Castelein et al.*, 2001; *Horváth et al.*, 2003], serpentinite [e.g., *Cattaneo et al.*, 2003; *Candela et al.*, 2007], and montmorillonite [e.g., *Huang et al.*, 1994; *Bray et al.*, 1998; *Bray and Redfern*, 1999]. These studies do not systematically present precise kinetic parameters that can directly be used in the model, mainly because the first-order rate law we chose does not always hold. However, all these experimental data highlight the fact that when heating rates are high, the reactions significantly start at higher temperatures and at faster kinetic. In particular, *Huang et al.* [1994] show that montmorillonite dehydration is of the order of minutes, and can be even faster for the release of the interlayer water [*Bray and Redfern*, 1999]. Likewise, *Candela et al.* [2007] report that the complete phase transition from chrysotile to forsterite can be achieved within 1–10 min when the samples are heated several hundreds of degrees above the equilibrium temperature.

[33] In order to have an insight of the potential relevance of dehydration effects in the framework of rapid slip events on a fault, we can compare the characteristic time of dehydration to the characteristic duration of an earthquake. From the Arrhenius law (equation (33)), we can calculate the temperature at which the kinetic constant κ becomes of the order of 1 s^{-1}. This temperature is plotted on Figure 3 as a function of E_a and T_s, for a constant value of $\kappa_s = 10^{-4}$ s^{-1}. Figure 3 highlights that dehydration reactions may last ~1 s at a temperature of ~900°C for kaolinite, ~1100°C for talc and ~670°C for lizardite.

[34] In the following, the rate constant κ will thus be calculated with equation (33), using an average $\kappa_s = 10^{-4}$ s^{-1} and $E_a = 300$ kJ mol^{-1}. These values have to be considered as global averages for most of the dehydration reactions of clays and serpentine. The starting temperature T_s now can be viewed as the real equilibrium temperature, because the temperature overstep will be directly handled by the Arrhenius law.

5. The General Case: Effects of Fluid and Heat Diffusion

[35] The adiabatic, undrained approximation described previously is an end-member, valid for small displacements and/or a relatively thick slipping zone [*Rempel and Rice*, 2006] only. In order to get a more realistic view of the system, it is important to take into account heat and fluid diffusion. This case can be solved numerically using the general equations (5) and (14) which are recalled here:

$$\frac{\partial T}{\partial t} = \mu(\sigma_n - \bar{p})\frac{V}{h\rho c} + \alpha_{th}\frac{\partial^2 T}{\partial y^2} + \frac{\Delta H}{\rho c}\frac{\partial \xi}{\partial t},$$
$$\frac{\partial p}{\partial t} = \Lambda\frac{\partial T}{\partial t} + \frac{1}{\rho_f \beta^*}\frac{\partial}{\partial y}\left(\rho_f \frac{k}{\eta_f}\frac{\partial p}{\partial y}\right) + \left(\frac{\rho}{\rho_f}\chi - \Delta n^{irr}\right)\frac{1}{\beta^*}\frac{\partial \xi}{\partial t}.$$

The reaction rate still needs to be calculated using the minimum between the kinetic constant $\kappa(\overline{T})$ and the energetically constrained rate. In order to take into account heat diffusion, equation (32) needs to be modified as follows:

$$\frac{\partial \xi}{\partial t} = \min\Big\{(1-\xi)\kappa\big(\overline{T}(t)\big), -\frac{1}{\Delta H}\left(\frac{\mu V(\sigma_n - \bar{p}(t))}{h} + \alpha_{th}\rho c\frac{\partial^2 T}{\partial y^2}\right)\Big\}. \quad (34)$$

The last term corresponds in fact to $-(1/\Delta T^d)(\partial T/\partial t)$, which means that all the thermal energy is driving the dehydration reaction.

5.1. Modeling Strategy

[36] Calculations are performed numerically using a one dimensional implicit finite difference scheme, with constant time steps and variable space steps (see Appendix A for details on the numerical discretization). Only one half-space is modeled, and a zero flux condition is set at both edges of the grid. The grid size is large enough to prevent border effects. This method allows to take into account the dependencies of some parameters on pressure and temperature. In particular, water properties are calculated using the IAPWS-IF97 data set and the GE0TAB software [*Berman*, 1991, 2007]. The values of all the parameters are summarized in Table 2.

5.2. Numerical Results

[37] Figure 4 shows two representative behaviors of the pore pressure, the temperature and the reaction extent within the slipping zone for two different starting temperatures T_s. The reference TP curve (gray line) is plotted for comparison. In the case when T_s = 500°C (dotted line), which corresponds to the dehydroxylation temperature of kaolinite, the reaction induces a slight increase in pore pressure and slows down the temperature increase. These two features are very similar to the adiabatic, undrained case. However, the kinetic of dehydration is different. Here, the rate constant κ_s when the reaction starts is set at 0.0001 s^{-1}, but κ is now also temperature dependent. The kinetic is thus faster, which induces nonnegligible effects due to the dehydration reaction.

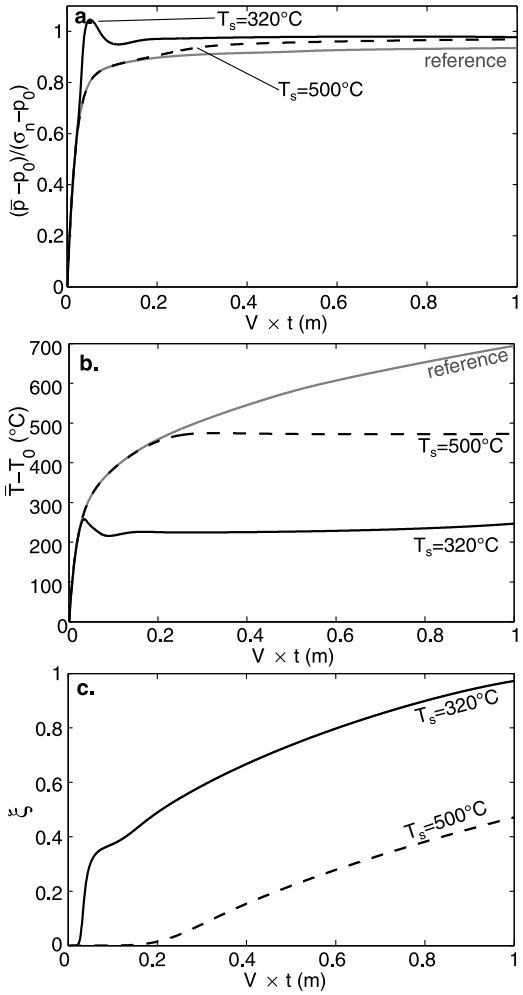

Figure 4. Numerical simulations including pore fluid and heat transport for permeability $k = 10^{-20}$ m^2. (a) Average pore pressure evolution within the slipping zone. (b) Average temperature evolution within the slipping zone. (c) Evolution of the reaction extent. The reference thermal pressurization curve is plotted in gray. The dashed curve corresponds to parameters values summarized in Table 2. The full black curve corresponds to the case of $T_s = 320$°C. In both cases, the temperature increase is stopped while the reaction is progressing. When the reaction is finished, it starts increasing again. In the case of a low dehydration temperature (full line), the pore pressure increases over the normal stress, and the reaction tends to progress faster.

[38] Because the Arrhenius law forbids the temperature to be much higher than the equilibrium temperature while the reaction is occurring, the reaction progresses at an almost constant temperature, slightly higher than T_s (~180°C overstep). As the equilibrium temperature is exceeded, the reaction rate increases and the system cools down because the reaction is endothermic. Figure 4c shows that the reaction rate is relatively low at the beginning of the dehydration and then increases at around 0.2 s, which corresponds to the time when the temperature increase is large enough to induce a large increase of $\kappa(\bar{t})$. From then on, the slip continues at a constant temperature and a transient equilibrium is met between energy production through frictional heating and energy dissipation through mineral dehydration.

[39] If the equilibrium temperature is lower ($T_s = 320$°C, which is approximately the dehydration temperature of smectite), the pore pressure increases abruptly at the onset of dehydration and can increase beyond the applied normal stress σ_n. This is possible because of the temperature overstep, which can be viewed as additional stored energy. This energy is absorbed by the reaction even if the frictional energy falls to zero. Subsequently, the pore pressure decreases slightly below σ_n but remains high while the dehydration reaction progresses. The average temperature remains very close to T_s. The reaction extent is fast at the beginning. During the transient overpressure, it almost stops and then reincreases when the pore pressure decreases below the normal stress again. This corresponds to a shift from the first order kinetic to the energy-controlled kinetic, which slows down the progress of the reaction. This is clearly linked to the way the reaction kinetic is calculated: it is bounded by the amount of energy available in the system and is low when friction $\mu(\sigma_n - \bar{p})$ is low.

[40] Figure 5 displays the same plots for a fault zone with a much higher permeability $k = 10^{-18}$ m^2. The reference TP curve (gray line) is plotted for comparison. Its shape is not monotonic due to the evolution of thermodynamic properties of water at high temperatures. Above 1200°C, melting is supposed to start and the curves are not plotted after this point (denoted by a star). For a low amount of water ($\chi = 0.01$), the dehydration reaction is almost instantaneous and triggers a pore pressure peak within the slipping zone. The average pore pressure then drops as the fluid diffuses outside the slipping zone. However, there is no significant effect on the average temperature.

[41] When the amount of water is 10 times greater ($\chi = 0.1$, solid line), the dehydration reaction also triggers a pore pressure pulse but the pore pressure is maintained at a high level while the reaction progresses. This can only be observed because the dehydration source term is of the same order of magnitude as the fluid diffusion term in equation (14). This important observation corresponds to the end-member case of pure chemical pressurization of the fault by mineral dehydration. It shows that fault rocks of higher permeabilities can be chemically pressurized. This could be of particular importance in damaged fault rocks where thermal pressurization alone is not effective. The pore pressure evolution plotted on Figure 5 can also be seen as the frictional shear stress on the fault. Therefore, we can infer that the shear stress increases immediately after the dehydration reaction is completed. This is an important observation as it points out that the completion of a given mineral dehydration could act as a frictional barrier. Concurrently, the temperature does not increase until the reaction is finished. Once the reaction is consumed, the average pore pressure starts decreasing and the average temperature increases again up to the melting point. Note that the slip distance required to reach the onset of melting is several times larger than the one required in the case of TP only.

5.3. Parametric Study of the Influence of Dehydration Reactions

[42] Here, we describe the relative importance of each parameter linked to the mineral reaction (starting tem-

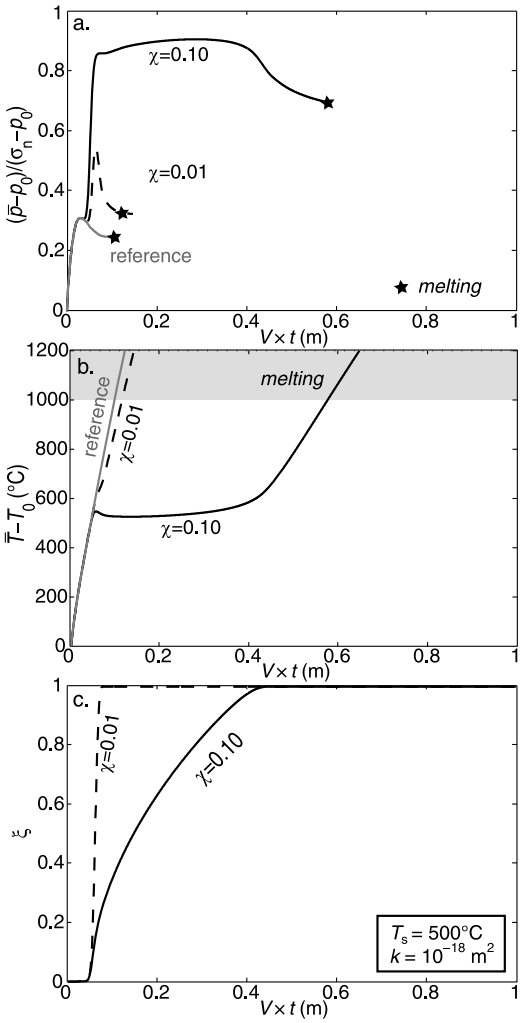

Figure 5. Numerical simulations including pore fluid and heat transport for permeability $k = 10^{-18}$ m^2. (a) Average pore pressure evolution within the slipping zone. (b) Average temperature evolution within the slipping zone. (c) Evolution of the reaction extent. The reference thermal pressurization curve is plotted in gray. Except for permeability, the parameter values are given in Table 2. The dashed curve corresponds to $\chi = 0.10$ (large water amount), and the full curve corresponds to $\chi = 0.01$ (low water amount). The curve for $\chi = 0.01$ displays a large pore pressure peak when dehydration occurs, and it drops almost immediately when the reaction is finished. In this case, the reaction is very fast, and no visible effect can be seen on temperature. For a large amount of water ($\chi = 0.1$), the pore pressure increases and is kept at a high value while the reaction is progressing. At the same time, the average temperature is kept close to T_s. When the reaction is finished, the temperature increases again, and the pore pressure decreases.

perature T_s, enthalpy variation ΔH, rate constant κ_s and activation energy E_a) as regards to the global thermo-hydrochemomechanical behavior of the slipping zone. All the simulations are performed with parameter values referenced on Table 2, except explicitly stated otherwise.

[43] Figure 6 presents the effect of the equilibirum temperature T_s, varying from 300°C to 800°C, and the total amount of water per unit volume χ on the temperature reached at one meter of slip (i.e., 1 s), the maximum pore pressure increase reached during slip Δp_{max} normalized to $\sigma_n - p_0$ and the extent of the reaction at one meter of slip (i.e., 1 s), respectively. Figure 6c shows that when both χ and T_s are low, the reaction is completed before the slip reaches 1 m. This corresponds to the regime denoted by "complete dehydration". As seen in section 5.2, the earlier the reaction is finished, the higher the temperature can be at 1 m slip. For higher values of χ or T_s, the reaction still progresses after 1 m slip and as a consequence, the final temperature is close to that of the mineral reaction starting temperature, with an average 100–150°C overstep. If T_s is low and χ is high, overpressures can occur, which is consistent with the observation made on Figure 4. This is due to the fact that the pore pressure is low at the onset of dehydration. Consequently, the frictional energy is high and the reaction kinetic is not bounded by the amount of energy available in the system, but is rather controlled by the first-order kinetic, which allows the pore pressure to exceed the normal stress.

[44] Similarly, Figure 7 presents the dependency on the enthalpy variation of the mineral reaction. As χ is involved in the calculation of ΔH, the ratio $|\Delta H/\chi|$ is used to avoid correlations between the two parameters investigated here. In the range $|\Delta H/\chi| = 10^9$ to 10^{11} J m^{-3} (corresponding to $\Delta_r H$ from 10 to 1000 kJ mol^{-1}), the behavior of the system is constant. Complete reactions are observed for low water contents (Figure 7c), for which larger temperatures are attained at 1 m of slip. No overpressure is observed. However, a similar plot for calculations performed at a lower T_s would show that overpressures can only occur at relatively low $|\Delta H/\chi|$ (of the order of 10^{10} kJ mol^{-1}). This is consistent with the fact that a reaction with a large enthalpy variation promotes an energy-controlled kinetic and thus cannot induce overpressures.

[45] Figure 8 presents the effect of the rate constant κ_s, for a wide range of values from 10^{-15} to 10^0 s^{-1}. When $\kappa_s > 10^{-2}$ s^{-1} and $\chi < 0.01$, dehydration reactions tend to be completed before the slip reaches 1 m. When $\kappa_s < 10^{-6}$ s^{-1}, Figure 8c shows that the reaction does not significantly progress: the effect of dehydration would thus be negligible. However, Figure 8a shows that the temperature at 1 m slip can be more than 400°C higher than the starting temperature whereas the reaction is not fully completed. This is physically unrealistic because such a temperature overstep would normally strongly accelerate the reaction by increasing the activation energy E_a. For the sake of simplicity we do not take into account such a dependency here and the calculations can thus be viewed as lower estimates.

[46] Finally, the value of activation energy E_a is investigated on Figure 9. If E_a is below 10^2 kJ mol^{-1}, the reaction kinetic is weakly dependent on temperature, which dramatically slows down the dehydration process: after 1 m slip, the extent of reaction is still less than 20% and the temperature overstep can be more than 300°C. Again, this situation is unrealistic and highlights a limit of our model which neglects the dependency of E_a on T. If the activation energy is larger than a few hundreds kilojoules per mole, which seems to be closer to experimental data, the temperature can be kept close to T_s while dehydration reactions are progressing and the pore pressure increase becomes significant.

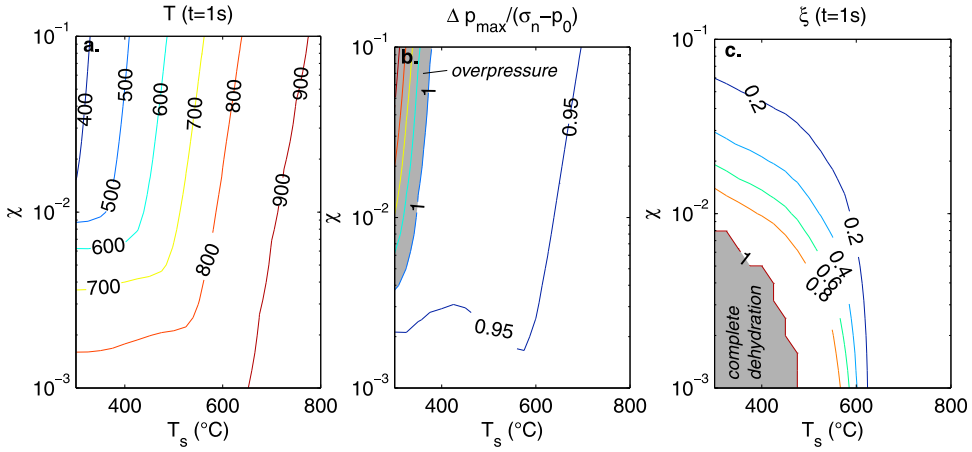

Figure 6. Dependency of (a) T at 1 s of slip, (b) maximum relative pore pressure increase $(p_{max} - p_0)/(\sigma_n - p_0)$, and (c) ξ at 1 s of slip on the total amount of water χ and the starting temperature T_s. Overpressures can develop at low T_s and high χ. When the reaction is not finished, the temperature is strongly controlled by T_s, which is a boundary for the temperature during the dehydration process.

5.4. Influence of Depth and Width of the Slipping Zone

[47] Parameters such as permeability k, slipping zone thickness h and the depth z at which the slip occurs, could also change the behavior of the system. The effect of permeability has already been discussed previously (Figure 5).

[48] Figure 10 shows the effects of a change in the slipping zone thickness h, ranging from 10^{-4} to 10^{-2} m, on the pore pressure, the temperature and the reaction extent. An ultrathin slipping zone promotes a faster dehydration since it increases the frictional energy (first term on the right-hand side of equation (5)) and decreases the total mass of water that is released per unit of fault area. The effect of dehydration is nonnegligible since there is a large temperature difference compared to regular TP (~150°C) even after dehydration is completed. However, Figure 10a displays only a slight increase in pore pressure during the reaction. If h is large, i.e., around 1 cm, the effect of dehydration is negligible because the temperature does not increase significantly over the starting temperature T_s.

[49] Finally, we investigate the dependency of the system on the depth at which the slip occurs. Figure 11 presents the temperature reached at one meter of slip (i.e., 1 s), the maximum pore pressure increase reached during slip Δp_{max} normalized to $\sigma_n - p_0$ and the extent of the reaction at one meter of slip (i.e., 1 s), as a function of depth and χ. A variation in depth corresponds to a change in the initial temperature T_0, pore pressure p_0 and normal stress σ_n. At a large depth, the initial temperature is closer to T_s, which enhances the possibility of overpressures (as seen on Figure 4). Indeed, Figure 11b shows that overpressures can occur when the depth is lower than 10 km and when the amount of water that can be released is higher than 1%. Figure 11a shows that a large depth also tends to increase the occurrence of melting (i.e., average temperature higher than 1200°C). This is con-

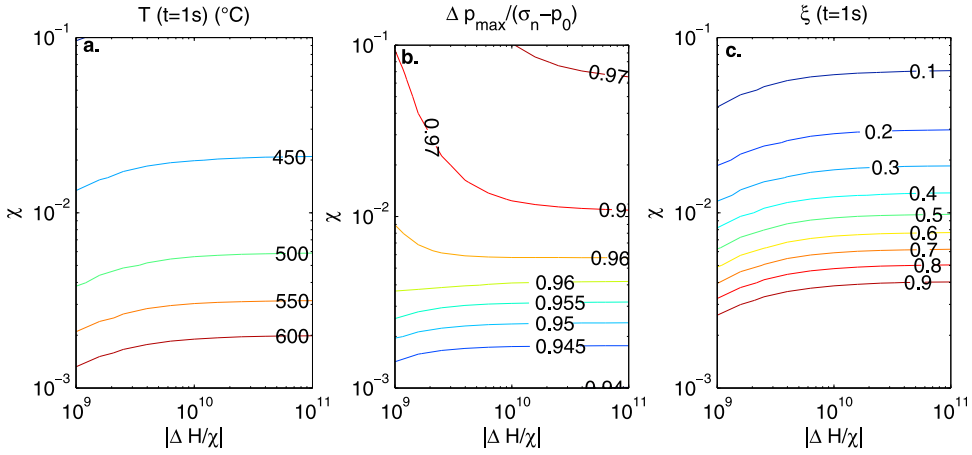

Figure 7. Dependency of (a) T at 1 s of slip, (b) maximum relative pore pressure increase $(p_{max} - p_0)/(\sigma_n - p_0)$, and (c) ξ at 1 s of slip on the total amount of water χ and the enthalpy change per unit of slipping zone volume $|\Delta H/\chi|$. The enthalpy of the reaction ΔH does not play an important role in the temperature and pressure evolution.

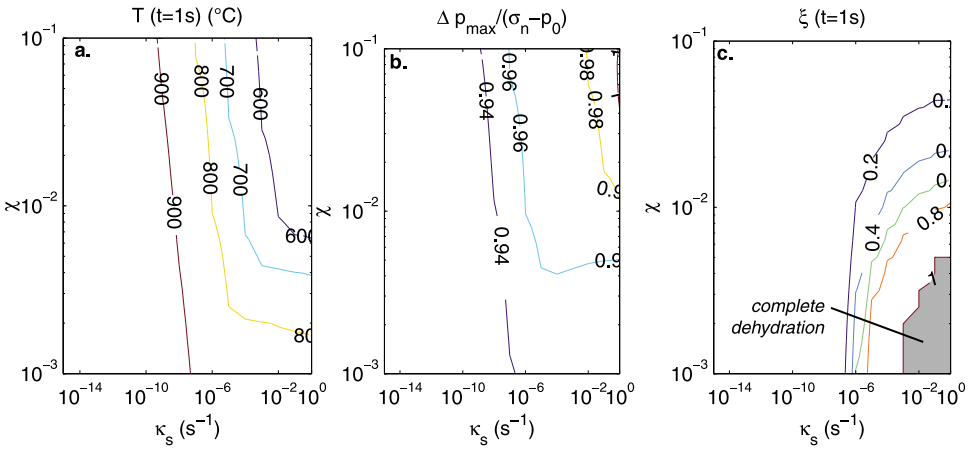

Figure 8. Dependency of (a) T at 1 s of slip, (b) maximum relative pore pressure increase $(p_{max} - p_0)/(\sigma_n - p_0)$, and (c) ξ at 1 s of slip on the total amount of water χ and the kinetics at the onset of dehydration κ_s. If the rate constant at equilibrium is very low (from 10^{-15} to 10^{-6} s^{-1}), the effect of dehydration becomes negligible, and the temperature can be much higher than the equilibrium temperature during the reaction. A large constant rate constant promotes small temperature oversteps compared to T_s and a high pore pressure increase.

sistent with theoretical results from *Rempel and Rice* [2006] and *Rice* [2006] which show that the temperature increase during thermal pressurization is directly proportional to $\sigma_n - p_0$. In addition, we show here that dehydration reactions occur very rapidly and are completed in less than 1 s at depths larger than 8 km and do not prevent the fault from melting, but just delay the time of its onset (as seen on Figure 5b). The overall behavior of the system seems to be controlled by the depth at which the slip occurs. In these simulations the starting temperature T_s is kept constant at 500°C; however, it is very likely that hydrous minerals occurring at small depth would not necessarily be the same as those occurring at large depth; that is, the starting temperature of each dehydration reaction would be changing with depth. Thus if $T_s > 500$°C, Figure 11 should be shifted toward the smaller depths, whereas if $T_s <$ 500°C, Figures 11a–11c should be shifted toward the larger depths. Variations of properties and minerals along the fault will be fully discussed in section 6.

6. Discussion

6.1. Implications of the Model

[50] Our analytical and numerical results have important implications. First, coseismic mineral dehydrations are shown to be an effective pressurization process when the fault rock contains a significant amount of water within the solid phase ($\chi \gtrsim 0.5\%$). In a previous study, *Brantut et al.* [2008] calculated some values of parameter χ for several known fault zones, showing that its value was mostly above 1% and up to 10% (in fault gouges from the SAFOD cores).

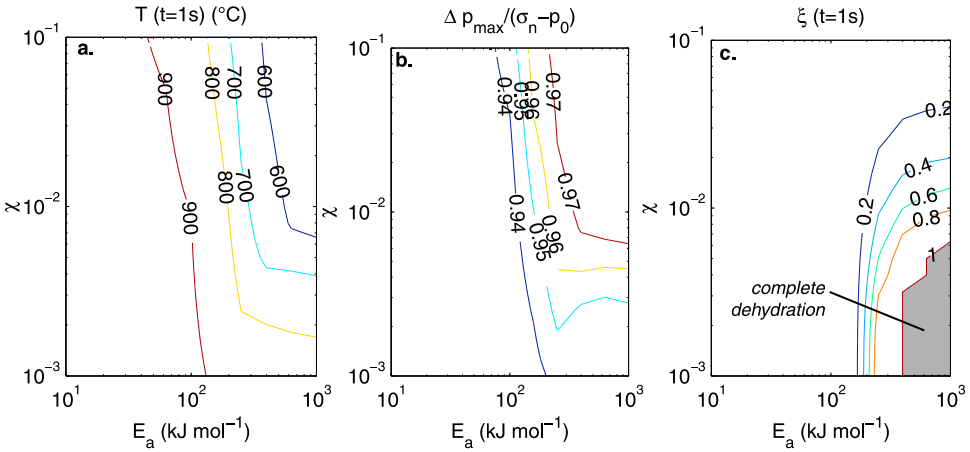

Figure 9. Dependency of (a) T at 1 s of slip, (b) maximum relative pore pressure increase $(p_{max} - p_0)/(\sigma_n - p_0)$, and (c) ξ at 1 s of slip on the total amount of water χ and the activation energy E_a. Other parameters are set at the values presented on Table 2. The activation energy strongly influences the system. At a low E_a, the temperature overstep can be very large (more than 350°C), and the reaction is very slow (ξ is less than 20%), thus promoting negligible pore pressure pulses.

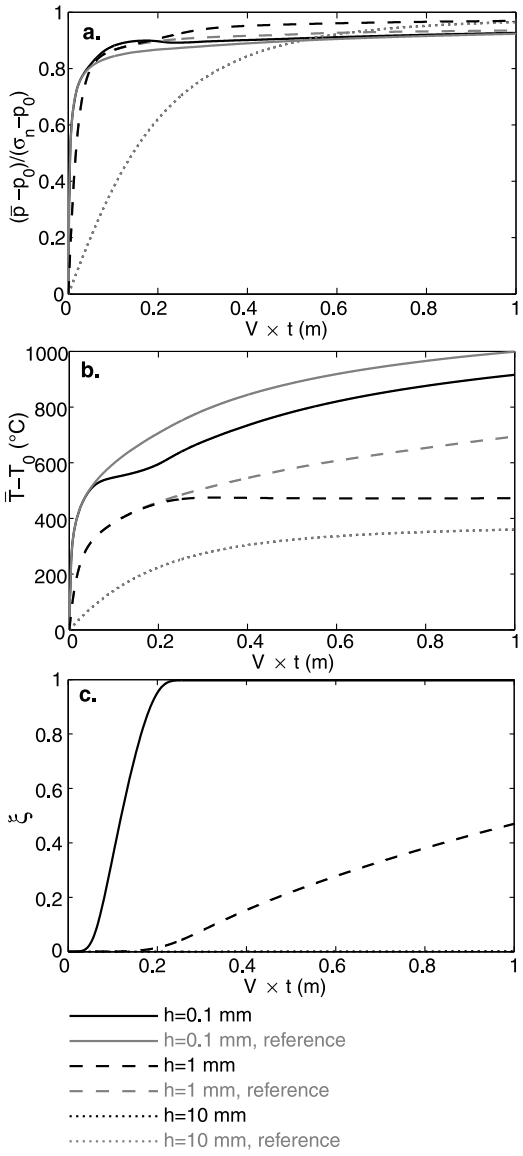

Figure 10. Numerical simulations including pore fluid and heat transport for various slipping zone width h = 0.1–1–10 mm. (a) Average pore pressure evolution within the slipping zone. (b) Average temperature evolution within the slipping zone. (c) Evolution of the reaction extent. The reference thermal pressurization curve is plotted in gray. The other parameters values are summarized in Table 2.

While the dehydration reaction progresses, the temperature remains close to the mineral reaction equilibrium temperature, or close to the starting temperature if an overstep is needed for the reaction to begin. This is due to both the thermoporoelastic coupling (factor Λ) and the latent heat of the mineral reaction (factor ΔH). Coseismic mineral dehydrations are thus a possible mechanism that may prevent or at least delay melting during rapid shear events on the fault. It is, however, important to note that dehydration reactions can be neglected if TP is very effective, i.e., if the temperature does not largely exceeds the dehydration temperature T_s or if the reaction kinetic is very slow ($\kappa_s < 10^{-6}$ s^{-1}). Another consequence of our results is that when a fault rock contains several mineral species that can dehydrate (or if one mineral can dehydrate successively at several temperature stages), then the temperature is likely to evolve by steps within the slipping zone, each of these steps corresponding to a particular dehydration reaction. In all cases, melting can occur only after all the hydrous minerals have been dehydrated, or only if the reaction rate is too small.

[51] When the equilibrium temperature of the mineral dehydration is low when compared to the initial temperature T_0 ($T_s - T_0 \lesssim 150$°C), the pore pressure can build up beyond the normal stress, which can never occur within the classical thermopressurization framework. In such cases, the fault would be frictionless, and the fault rock can experience a transient tension, likely to trigger hydrofracturing and damage in the fault walls. In particular, such low dehydration temperatures may correspond to clay minerals prevalent in shallow fault gouges such as smectites, illite, montmorillonite [*Mizoguchi*, 2005; *Solum et al.*, 2006], which are known to contain a large amount of water. In addition, grain crushing and comminution usually occurring during coseismic slip may also lower the equilibrium temperatures at which mineral dehydrations take place [*Makó et al.*, 2001; *Horváth et al.*, 2003]. It is also important to note that if an earthquake propagates within a zone where hydrous minerals are close to their dehydration temperature then, for the reason stated above, overpresssures are more likely to occur.

[52] For fault rocks with higher permeability for which classical TP would be inefficient, our results highlight that a pure chemical pressurization of the fault may happen and the pore fluid can be transiently pressurized because of mineral dehydration only. Note, however, that if the dehydration kinetic is too slow (e.g., $\kappa \sim 10^{-10}$ s^{-1}), the simulations lead to melting before the onset of dehydration, because the temperature overstep is not high enough to make the reaction significantly progress. Once the reaction is completed, the pore pressure drops due to fluid diffusion, which also corresponds to an increase in frictional shear stress. Mineral dehydration completeness corresponds to a nonmonotonic evolution of frictional shear stress with increasing slip and the generation of frictional barriers. Since it is likely that if the slip rate also evolves as a function of frictional stress, such an increase in friction may induce a decrease of the slip velocity or even stop the slip event.

[53] Our numerical results also demonstrate that the thickness of the slipping zone plays an important role, as it changes the heating rate and the maximum temperature the system can reach due to TP. In the case of a thin slipping zone $h < 0.1$ mm, mineral dehydrations are very rapid but the pore pressure and temperature are not much altered. However, our model is limited in the sense that it allows dehydration within the slipping zone only. A more complete description would allow for the mineral dehydrations to take place anywhere within the fault zone, depending on the temperature reached at each location across the fault. Such a model could be an effective way to describe the relationship between the thickness evolution of the dehydration zone and the total amount of displacement. It is likely that melting would be even rarer in this situation because dehydration will progress outside the slipping zone and diffusion of pore pressure and temperature will lower the overall temperature of the system.

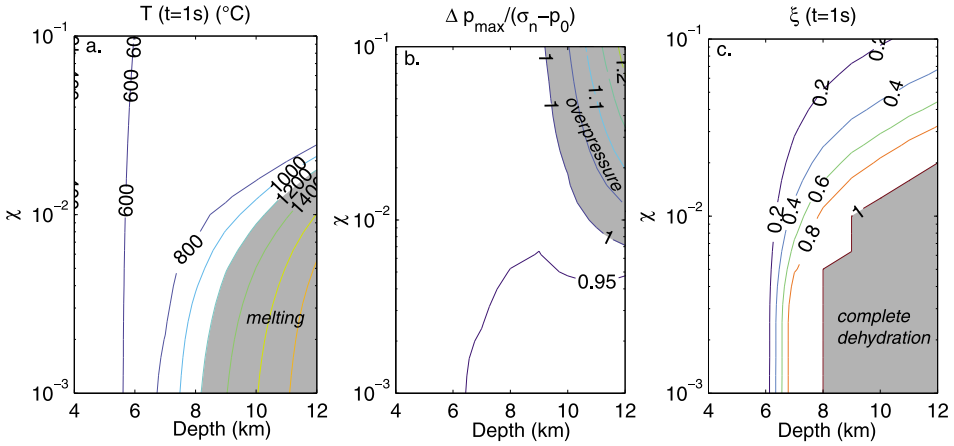

Figure 11. Dependency of (a) T at 1 s of slip, (b) maximum relative pore pressure increase $(p_{max} - p_0)/(\sigma_n - p_0)$, and (c) ξ at 1 s of slip on the total amount of water χ and depth. Other parameters are set at the values presented in Table 2. The melting temperature is set at 1200°C. A variation in depth corresponds to a change in initial conditions (normal stress, pore pressure, and temperature). A large depth (>8 km) promotes large temperature increases (including melting). With χ 0.01, overpressures can occur, but melting will not occur, at least while dehydration is not finished.

[54] Judging from Figure 11, the depth at which the slip occurs strongly controls the mechanical behavior of the system, in particular the possibility of overpressures and melting. Complete mineral dehydrations seem to prevail at depth along with overpressures and fluidization. Each depth might correspond to a given set of hydrous minerals: at shallow depths, clays such as smectite, illite or montmorillonite are likely to play an important role. For deeper faults, hydrous phyllosilicates such as chlorite, talc or serpentinite may become important. This emphasizes the importance of the mineral composition of the fault rocks. This is consistent with observations made on samples from the Chelung-Pu drill cores that display strong changes in clay amounts between the bulk rock and the fault gouges [*Hirono et al.*, 2008]. Such observations may help building thermometers for natural faults gouges but experimental and theoretical work is still much needed to constrain the precise temperatures reached along a fault during an earthquake.

6.2. Limitations of the Model

[55] Except for the dehydration kinetic, the equations developed here do not depend on any particular dehydration mechanism. Only slight modifications would be needed to take into account the release of interlayered water. Our model could also be applied to fault rocks undergoing coseismic decarbonation. The theoretical framework is indeed very close to that developed by *Sulem and Famin* [2009]. Seismic decarbonation has been observed on fault zones after real earthquakes [e.g., *Famin et al.*, 2008]. Although in such a case the properties of the fluid (compressibility, thermal expansion and density) are very different, there is still a mechanical effect due to carbonate degassing.

[56] There were problems in finding a relevant, precise parameter set for this model. On one hand, for a particular chemical reaction, the equilibrium temperature and the enthalpy variation are precisely given by experimental thermodynamical studies. On the other hand, however, the kinetic parameters for our study are hard to constrain because there is a clear lack of data available for extremely fast heating rates (of the order of several hundreds of degrees per second). Our investigation on the parameters κ_s and E_a highlights that the reaction needs to be fast and strongly temperature-dependent to produce a significant effect on the overall pressure and temperature of the system. This might be due to the fact that the activation energy is a constant in our description. A more complete description would actually include the Gibbs free energy variation ΔG. This would enhance the overall dependency of the reaction kinetic on temperature and thus limit the temperature overstep during the reaction. However, such detailed calculations are beyond the scope of this study which aims at giving elementary estimates based on a restricted number of parameters.

[57] The permeability and storage capacity values used in the calculations come from static measurements at a given effective pressure and temperature [e.g., *Wibberley and Shimamoto*, 2003]. Strain is known to have great influence on those rock properties: it is thus very likely that they can be different during a very rapid slip event compared to their static measurement in the laboratory. However, it is difficult to estimate intuitively whether the laboratory values used in this study are a lower or an upper bound of the in situ values.

[58] The simulations were performed at a constant slip velocity $V = 1$ m s^{-1}. It is important to mention that the results are not only slip dependent, i.e., Vt, but also slip rate dependent. For instance, heat loss by diffusion will be reduced for faster slip rates and the temperature will tend to be higher after equal slip amounts. A simple way to investigate this effect is to recognize that the slip velocity V appears in the strain rate $\dot{\epsilon} = V/h$. Thus a variation in V produces the inverse effect of a variation in h. However, this mathematical point of view is too simplistic since the slip rate is highly variable during an earthquake. Such variations were not investigated here.

[59] Finally, the approximation of no solid volume change during the reaction needs to be discussed. At low pressures (a couple of hundreds of MPa), mineral dehydration reactions are always accompanied with an increase of the total volume (i.e., the solid volume reduction is small compared to the volume taken by the fluid phase), so that the sign of the pore pressure variation generated by the reaction Δp^{irr} is always positive. Here, we assumed that the solid volume change induced by the reaction was either negligible, or could be simply modeled by a lower amount of water χ contained in the solid phases. This is an important simplification, because the negative solid volume change due to the reaction induces an increase in porosity, which in turn induces an increase in the storage capacity β^* (equation (10)). Note that the storage capacity β^* will never increase by more than an order of magnitude due to such an increase of porosity (a maximum variation of ~10%). In addition, if the permeability is not modified, an increase in storage capacity also results in a decrease in fluid diffusivity, implying a stronger pressurization effect. In the opposite way, an increase in porosity also tends to induce an increase in permeability by generating new connecting pathways for the fluid. Such phenomena are difficult to take into account, which is the reason why we chose not to tackle these problems.

[60] Even with these elementary simplifications, the number of independent parameters still remains very high. The most important ones are unfortunately also those that are the less constrained by experimental and field data, such as the thickness of the slipping zone and the reaction kinetics. All the parameters are also not constant along a fault, and the behavior of the system will be different from one place to another. It is thus of primary importance to collect more data on natural fault zones to constrain the mechanical behavior of natural faults during coseismic slip.

7. Conclusions

[61] In summary, our work introduces a thermo-hydrochemical coupling to the formulation of thermal pressurization of faults. This coupling consists in the coseismic triggering of mineral dehydration reactions, which have been observed both experimentally during high velocity friction experiments [*Hirose and Bystricky*, 2007; *Brantut et al.*, 2008] and in the field [*Hirono et al.*, 2008; *Famin et al.*, 2008; *Hamada et al.*, 2009]. When the dehydration temperature is low enough and the dehydration kinetic fast enough, which is the case for most hydrous clays and phyllosilicates, this phenomenon cannot be neglected and will result in a more complex behavior of the fault zone in term of pore pressure and temperature evolution during slip. Indeed, we show that the fault rock may undergo transient overpressures. An important point of our study is that the temperature rise in the slipping zone is stopped while the dehydration reaction progresses. This highlights the fact that in our case, an equilibrium is met during slip between energy release by frictional heating and energy dissipation by mineral reaction. Our results also suggest that melting can be delayed when hydrous minerals are present within the fault rock, and that the coseismic mechanical behavior of a fault can be strongly influenced by its mineralogy. Our description could be improved by adding precise kinetic parameters and by taking into account the dependency of some parameters (such as for example porosity, permeability reaction activation energy) on pore pressure, stress and temperature. This last point highlights the current lack of complete experimental data sets on natural fault rocks.

Appendix A: Modeling Strategy

[62] The discretization of our numerical model is based on constant time steps denoted Δt and variable space steps denoted Δy_i. The subscript i denotes the index of the space step and the superscript n denotes the time step. The index of the last grid within the slipping zone is called i_{sz}. Because of the symmetry of the problem, only one half-space is modeled. In all simulations, half of the slipping zone is divided into 10 space steps and the matrix is divided into decreasing space steps as the distance to the center increases. The boundary condition at the edge is zero heat and fluid flux and the total size of the grid is large enough to avoid any boundary effect. The numerical scheme inside the slipping zone can be written as follows:

$$\frac{T_i^{n+1}-T_i^n}{\Delta t}=\mathcal{T}_{\mathrm{th}}^{n+1}+\frac{\Delta H}{\rho c}\mathcal{X}^{n+1}+\frac{\mu V}{\rho c h}\left(\sigma_{\mathrm{n}}-\frac{1}{h/2}\sum_{i=1}^{i_{\mathrm{sz}}}\Delta y_i p_i^{n+1}\right), \tag{A1}$$

$$\frac{p_i^{n+1}-p_i^n}{\Delta t}=\mathcal{T}_{\mathrm{hy}}^{n+1}+\Lambda^n\frac{T_i^{n+1}-T_i^n}{\Delta t}+\Delta p^{\mathrm{d}}\mathcal{X}^{n+1}, \tag{A2}$$

where $\mathcal{T}_{\mathrm{th}}$ and $\mathcal{T}_{\mathrm{hy}}$ correspond to heat and fluid transport terms, respectively, and $\mathcal{X}$ corresponds to the dehydration term. Outside the slipping zone, the last term of equation (A1) is zero. The heat transport term is calculated implicitly with temperature, using constant diffusivity:

$$\mathcal{T}_{\mathrm{th}}^{n+1}=\alpha_{\mathrm{th}}\left[2\frac{T_{i+1}^{n+1}-T_i^{n+1}}{\Delta y_i(\Delta y_i+\Delta y_{i+1})}-2\frac{T_i^{n+1}-T_{i-1}^{n+1}}{\Delta y_i(\Delta y_i+\Delta y_{i-1})}\right]. \tag{A3}$$

The fluid transport term is implicit with respect to pressure, but includes diffusivity coefficients that are calculated explicitly, i.e., from the previous time step:

$$\mathcal{T}_{\mathrm{hy}}^{n+1}=\frac{1}{\rho_{\mathrm{f}i}^n\beta_i^{*n}}\left[2\frac{d_{i+1}^n\left(p_{i+1}^{n+1}-p_i^{n+1}\right)}{\Delta y_i(\Delta y_i+\Delta y_{i+1})}-2\frac{d_i^n\left(p_i^{n+1}-p_{i-1}^{n+1}\right)}{\Delta y_i(\Delta y_i+\Delta y_{i-1})}\right], \tag{A4}$$

where d_i^n is the hydraulic conductivity at the edge of grid i, calculated from the conductivity $(K_{\mathrm{hy}})_i^n$ inside the grid (Figure A1):

$$d_i^n=\frac{(K_{\mathrm{hy}})_{i-1}^n(K_{\mathrm{hy}})_i^n(\Delta y_{i-1}+\Delta y_i)}{(K_{\mathrm{hy}})_{i-1}^n\Delta y_i+(K_{\mathrm{hy}})_i^n\Delta y_{i-1}}, \tag{A5}$$

where

$$(K_{\mathrm{hy}})_i^n=\rho_{\mathrm{f}i}^n\frac{k_i^n}{\eta_i^n}. \tag{A6}$$

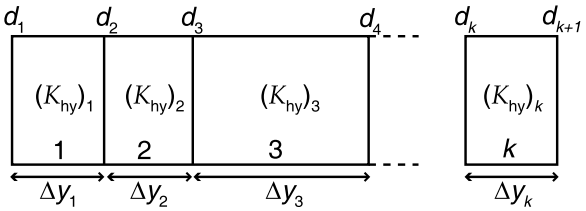

Figure A1. Discretization with nonconstant space steps. The equivalent diffusivity d_k at the border of grids k and $k-1$ is calculated from conductivity K_{hy} inside the corresponding grids through equation (A5).

The dehydration term $\mathcal{X}$ is calculated at the end of each time step, depending on the process that drives the reaction kinetic (following equation (32)). The corresponding pressure and temperature changes are taken into account after this calculation. At the end of a time step, if the average temperature $\overline{T}$ is higher than T_s, then ξ^{n+1} is calculated as follows:

$$\frac{\xi^{n+1}-\xi^n}{\Delta t}=\min\left\{\kappa\left(\overline{T}^n\right)\left(1-\xi^{n+1}\right),\frac{\overline{T}^n-T_s}{\Delta H/(\rho c)}\right\}, \qquad \text{(A7)}$$

where the rate constant κ is explicit with respect to temperature. The first case corresponds to a first-order reaction kinetic. In the second case, the reaction progress is calculated using energy balance, leading automatically to $\overline{T}^n = T_s$ at the end of the time step.

[63] **Acknowledgments.** The authors thank F. Brunet, Y. Guéguen, and J. Sulem for helpful discussions and suggestions. An anonymous reviewer helped us by pointing out the importance of reaction kinetics in our model. The authors are also grateful to two other anonymous reviewers who helped in improving the global readability of the manuscript.

References

Andrews, D. J. (2002), A fault constitutive relation accounting for thermal pressurization of pore fluid, *J. Geophys. Res.*, *107*(B12), 2363, doi:10.1029/2002JB001942.

Bellotto, M., A. Gualtieri, G. Artioli, and S. M. Clark (1995), Kinetic study of the kaolinite-mullite reaction sequence. Part I: Kaolinite dehydroxylation, Phys. *Chem. Miner.*, *22*, 207–214, doi:10.1007/BF00202253.

Berman, R. G. (1991), Thermobarometry using multi-equilibrium calculations: A new technique, with petrological applications, *Can. Mineral.*, *29*(4), 833–855.

Berman, R. G. (2007) winTWQ (version 2.3): A software package for performing internally-consistent thermobarometric calculations, *Geol. Surv. Can. Open File Rep., 5462*, 41 pp.

Bose, K., and J. Ganguly (1994), Thermogravimetric study of the dehydration kinetics of talc, *Am. Mineral.*, *79*, 692–699.

Brantut, N., A. Schubnel, J.-N. Rouzaud, F. Brunet, and T. Shimamoto (2008), High velocity frictional properties of a clay-bearing fault gouge and implications for earthquake mechanics, *J. Geophys. Res.*, *113*, B10401, doi:10.1029/2007JB005551.

Bray, H. J., and S. A. T. Redfern (1999), Kinetics of dehydration of Ca-montmorillonite, *Phys. Chem. Miner.*, *26*, 591–600, doi:10.1007/s002690050223.

Bray, H. J., S. A. T. Redfern, and S. M. Clark (1998), The kinetics of dehydration in Ca-montmorillonite: An in situ x-ray synchrotron study, *Mineral. Mag.*, *62*, 647–656, doi:10.1180/002646198548034.

Candela, P. A., C. D. Crummett, D. J. Earnest, M. R. Frank, and A. G. Wylie (2007), Low-pressure decomposition of chrysotile as a function of time and temperature, *Am. Mineral.*, *92*, 1704–1713, doi:10.2138/am.2007.2559.

Castelein, O., B. Soulestin, J.-P. Bonnet, and P. Blanchart (2001), The influence of heating rate on the thermal behaviour and mullite formation from a kaolin raw material, *Ceram. Int.*, *27*, 517–522, doi:10.1016/S0272-8842(00)00110-3.

Cattaneo, A., A. F. Gualtieri, and G. Artioli (2003), Kinetic study of the dehydroxylation of chrysotile asbestos with temperature by in situ XRPD, *Phys. Chem. Miner.*, *30*, 177–183, doi:10.1007/s00269-003-0298-2.

Di Toro, G., T. Hirose, S. Nielsen, G. Pennacchioni, and T. Shimamoto (2006), Natural and experimental evidence of melt lubrication of faults during earthquakes, *Science*, *311*, 647–649, doi:10.1126/science.1121012.

Famin, V., S. Nakashima, A.-M. Boullier, K. Fujimoto, and T. Hirono (2008), Earthquakes produce carbon dioxide in crustal faults, *Earth Planet. Sci. Lett.*, *265*, 487–497, doi:10.1016/j.epsl.2007.10.041.

Goguel, J. (1969), Le rôle de l'eau et de la chaleur dans les phénomènes tectoniques, *Rev. Geogr. Phys. Geol. Dyn.*, *11*, 153–163.

Goldsby, D. L., and T. E. Tullis (2002), Low frictional strength of quartz rocks at subseismic slip rates, *Geophys. Res. Lett.*, *29*(17), 1844, doi:10.1029/2002GL015240.

Hamada, Y., T. Hirono, W. Tanikawa, W. Soh, and S. Song (2009), Energy taken up by co-seismic chemical reactions during a large earthquake: An example from the 1999 Taiwan Chi-Chi earthquake, *Geophys. Res. Lett.*, *36*, L06301, doi:10.1029/2008GL036772.

Han, R., T. Shimamoto, J. Ando, and J. Ree (2007a), Seismic slip record in carbonate-bearing fault zones: an insight from high-velocity friction experiments on siderite gouge, *Geology*, *35*(12), 1131–1134, doi:10.1130/G24106A.1.

Han, R., T. Shimamoto, T. Hirose, J. Ree, and J. Ando (2007b), Ultra-low friction of carbonate faults caused by thermal decomposition, *Science*, *316*(5826), 878–881, doi:10.1126/science.1139763.

Hirono, T., et al. (2008), Clay mineral reactions caused by frictional heating during an earthquake: An example from the Taiwan Chelungpu fault, *Geophys. Res. Lett.*, *35*, L16303, doi:10.1029/2008GL034476.

Hirose, T., and M. Bystricky (2007), Extreme dynamic weakening of faults during dehydration by coseismic shear heating, *Geophys. Res. Lett.*, *34*, L14311, doi:10.1029/2007GL030049.

Hirose, T., and T. Shimamoto (2005), Growth of molten zone as a mechanism of slip weakening of simulated faults in gabbro during frictional melting, *J. Geophys. Res.*, *110*, B05202, doi:10.1029/2004JB003207.

Horváth, E., R. L. Frost, E. Makó, J. Kristóf, and T. Cseh (2003), Thermal treatment of mechanochemically activated kaolinite, *Thermochim. Acta*, *404*, 227–234, doi:10.1016/S0040-6031(03)00184-9.

Huang, W.-L., W. A. Bassett, and T.-C. Wu (1994), Dehydration and hydration of montmorillonite at elevated temperatures and pressures monitored using synchrotron radiation, *Am. Mineral.*, *79*, 683–691.

Kissinger, H. E. (1956), Variation of peak temperature with heating rate in differential thermal analysis, *J. Res. Natl. Bur. Stand. U.S.*, *57*(4), 217–221.

Klevtsov, D. P., V. A. Logvinenko, B. P. Zolotovskii, O. P. Krivoruchko, and R. A. Buyanov (1988), Kinetics of kaolinite dehydration and its dependence on mechanochemical activation, *J. Therm. Anal.*, *33*, 531–535, doi:10.1007/BF01913933.

Lachenbruch, A. H. (1980), Frictional heating, fluid pressure, and the resistance to fault motion, *J. Geophys. Res.*, *85*, 6097–6112, doi:10.1029/JB085iB11p06097.

Llana-Fúnez, S., K. H. Brodie, E. H. Rutter, and J. C. Arkwright (2007), Experimental dehydration kinetics of serpentinite using pore volumometry, *J. Metamorphic Geol.*, *25*, 423–438, doi:10.1111/j.1525-1314.2007.00703.x.

L'vov, B. V., and V. L. Ugolkov (2005), Kinetics and mechanism of dehydration of kaolinite, muscovite and talc analyzed thermogravimetrically by the third-law method, *J. Therm. Anal. Calorim.*, *82*, 15–22, doi:10.1007/s10973-005-0886-0.

Makó, E., L. Frost, J. Kristóf, and E. Horváth (2001), The effect of quartz content on the mechanochemical activation of kaolinite, *J. Colloid Interface Sci.*, *244*, 359–364, doi:10.1006/jcis.2001.7953.

Mase, C. W., and L. Smith (1985), Pore-fluid pressures and frictional heating on a fault surface, *Pure Appl. Geophys.*, *122*, 583–607, doi:10.1007/BF00874618.

Mizoguchi, K. (2005), High-velocity frictional behavior of Nojima fault gouge and its implications for seismogenic fault motion, Ph.D. thesis, Kyoto Univ., Kyoto.

Mizoguchi, K., T. Hirose, T. Shimamoto, and E. Fukuyama (2009), High-velocity frictional behavior and microstructure evolution of fault gouge obtained from Nojima fault, southwest Japan, *Tectonophysics*, *471*(3–4), 285–296, doi:10.1016/j.tecto.2009.02.033.

Noda, H., and T. Shimamoto (2005), Thermal pressurization and slip-weakening distance of a fault: An example of Hanaore fault, southwest Japan, *Bull. Seismol. Soc. Am.*, *95*(4), 1224–1233, doi:10.1785/0120040089.

Rempel, A., and J. R. Rice (2006), Thermal pressurization and onset of melting in fault zones, *J. Geophys. Res.*, *111*, B09314, doi:10.1029/2006JB004314.

Rice, J. R. (2006), Heating and weakening of faults during earthquake slip, *J. Geophys. Res.*, *111*, B05311, doi:10.1029/2005JB004006.

Sibson, R. H. (1973), Interaction between temperature and pore-fluid pressure during earthquake faulting—A mechanism for partial or total stress relief, *Nature*, *243*, 66–68.

Solum, L. G., S. H. Hickman, D. A. Lockner, D. E. Moore, B. A. van der Pluijm, A. M. Schleicher, and J. P. Evans (2006), Mineralogical characterization of protolith and fault rocks from the SAFOD main hole, *Geophys. Res. Lett.*, *33*, L21314, doi:10.1029/2006GL027285.

Sulem, J., and V. Famin (2009), Thermal decomposition of carbonates in fault zones: Slip-weakening and temperature-limiting effects, *J. Geophys. Res.*, *114*, B03309, doi:10.1029/2008JB006004.

Sulem, J., I. Vardoulakis, H. Ouffroukh, M. Boulon, and J. Hans (2004), Experimental characterization of the thermo-poro-mechanical properties of the Aegean fault gouge, *C. R. Geosci.*, *336*(4–5), 455–466, doi:10.1016/j.crte.2003.12.009.

Sulem, J., P. Lazar, and I. Vardoulakis (2007), Thermo-poro-mechanical properties of clayey gouge and application to rapid fault shearing, *Int. J. Numer. Anal. Methods Geomech.*, *31*, 523–540, doi:10.1002/nag.584.

Tsutsumi, A., and T. Shimamoto (1997), High-velocity frictional properties of gabbro, *Geophys. Res. Lett.*, *24*, 699–702, doi:10.1029/97GL00503.

Wibberley, C. A. J. (2002), Hydraulic diffusivity of fault gouge zones and implications for thermal pressurization during seismic slip, *Earth Planets Space*, *54*, 1153–1171.

Wibberley, C. A. J., and T. Shimamoto (2003), Internal structure and permeability of major-lip fault zones: The median tectonic line in Mie prefecture, southwest Japan, *J. Struct. Geol.*, *25*, 59–78, doi:10.1016/S0191-8141(02)00014-7.

Wibberley, C. A. J., and T. Shimamoto (2005), Earthquake slip weakening and asperities explained by thermal pressurization, *Nature*, *436*, 689–692, doi:10.1038/nature03901.

Wong, T.-F., S.-C. Ko, and D. L. Olgaard (1997), Generation and maintenance of pore pressure excess in a dehydrating system: 2. Theoretical analysis, *J. Geophys. Res.*, *102*(B1), 841–852, doi:10.1029/96JB02484.

Yeskis, D., A. F. Koster van Groos, and S. Guggenheim (1985), The dehydroxylation of kaolinite, *Am. Mineral.*, *70*, 159–164.

N. Brantut, J. Corvisier, and A. Schubnel, Laboratoire de Géologie, École Normale Supérieure, 24 rue Lhomond, F-75231 Paris CEDEX 05, France. (nicolas.brantut@ens.fr)

J. Sarout, CSIRO Division of Petroleum Resources, Australian Petroleum Co-operative Research Centre, ARRC, 26 Dick Perry Ave., Technology Park, Kensington, WA 6151, Australia.